Electronic Supplementary Information

Greatly Enhanced Mechanical Properties and Heat Distortion Resistance of Poly(L-lactic acid) Upon Compositing with Functionalized Reduced Graphene Oxide

Pengpeng Chen, Yuan Wang, Teng Wei, Zhen Meng, Xudong Jia,* and Kai Xi*

State Key Laboratory of Coordination Chemistry

Nanjing National Laboratory of Microstructures

Department of Polymer Science and Engineering

Nanjing University, Nanjing 210093, PR China

Xudong Jia *E-mail: jiaxd@nju.edu.cn.   Kai Xi *E-mail: xikai@nju.edu.cn.

1. Experimental

1.1. Materials

Graphite powder (99.99995%, 100 mesh) was purchased from Alfa Aesar. N-(2-aminoethyl)-3-aminopropyltrimethoxysilane was purchased from Liyang Mingtian Chemical Engineering Co., Ltd. H_2O_2 (30%) and N, N-dimethylformamide (DMF) were analytically pure and obtained from Sinopharm Chemical Reagent Co., Ltd. P_2O_5, $K_2S_2O_8$, $KMnO_4$, H_2SO_4, and hydrazine hydrate were analytically pure and obtained from Nanjing Chemical Reagent Co., Ltd. PLLA (M_w=120,000) was synthesized following the method reported by Jiang W *et al.*, in which isotactic polycondensation of L-lactic acid was catalyzed by biogenic creatinine.[1] All these reagents were used as received.

1.2. Preparation of RGO and KH792 modified RGO (KH792-RGO)

GO was firstly prepared by modified Hummers method.[2] The synthesized GO was purified by washing with deionized water and centrifuged successively three times, and suspended in deionized water by ultrasonication. The GO suspension was frozen dried to obtain the GO powders. 0.1 g of GO powders was dispersed in 200 mL of DMF via ultrasonication for 0.5 h. 0.2 g of KH792 was then added to the GO dispersion and the mixture was stirred at 80 ^{o}C for 10 h to get the KH792-GO. The resultant was filtrated and washed by DMF successively three times to remove the excess KH792. KH792-GO suspension was obtained after washing and dispersed in 200 mL of DMF by ultrasonication for another 30 min. 0.2 g of hydrazine hydrate was then added into the dispersion to reduce KH792-GO at 90 ^{o}C for 24 h. Finally the

reaction mixture was filtrated and washed by DMF successively three times to obtain KH792-RGO. The product was dispersed in DMF by ultrasonication and the concentration was measured. The RGO suspension with non-modification was also prepared. Without addition of 0.2 g of KH792, the GO mixture was reduced by hydrazine hydrate directly.

1.3. Preparation of PLLA/KH792-RGO composite

To prepare the nanocomposites, PLLA was firstly dissolved in DMF with a concentration of 25 wt%, followed by KH792-RGO suspension with a selected concentration added into the PLLA/DMF solution. The mixture was then stirred for 2 h and poured into a PTFE plate to remove the solvent at 80 $^{\circ}$C for 6 h. The samples were finally dried under vacuum at 120 $^{\circ}$C for 48 h. The PLLA/KH792-RGO nanocomposites with remarkable enhancement of mechanical properties and heat distortion resistance were obtained.

1.4. Characterization

The Fourier transform infrared spectra (FTIR) were recorded on a NICOLET NEXUS 870 spectrophotometer at room temperature in the 400-4000 cm^{-1} region.

Thermal gravimetric analysis (TGA) was examined using a Perkin-Elmer TGA-7 thermo gravimetric analyzer. Samples (2 mg) were loaded in platinum pans and measured from 25 to 700 $^{\circ}$C under a nitrogen environment at a heating rate of 20 $^{\circ}$C/min.

Transmission electron microscopy (TEM, JEM-2100) was carried out to study the morphologies. For RGO and KH792-RGO, one drop of the suspension was placed on

the sample grid, and the solvent was allowed to evaporate. For the nanocomposites, the samples were embedded in epoxy resin, and ultra-thin sections were made by using a Leica ULTRACUT UC6 with tens of nanometers thick. The sections were collected onto copper grids and then imaged at 200 kV.

X-ray photoelectron spectroscopy (XPS) (VG Microtech 2000 ESCA) was performed using a monochromatized Al Kα X-ray source (1486.6 eV).

Wide-angle X-ray diffraction (WAXD) patterns were recorded in transmission with a Bruker D8 Advance X-ray diffractometer. The wavelength used was Cu Kα (λ = 0.154 nm), and spectra were recorded in the 2θ range of 4–40° (step size 0.01°).

Morphologies of nanocomposite were also examined using a scanning electron microscopy (SEM, Hitachi S-4800). Samples were prepared by cryogenic fracture to observe a representative section (cross-section). An accelerating voltage of 10 kV with an Au coating of the sample was used to image the sections.

Rheology measurements were performed on HAAKE Rheo-Stress 600 rheometer at 200 °C, using a set of 20 mm diameter parallel plates with a sample thickness of ca. 0.7 mm.

The dynamic mechanical tests were carried out on a dynamic mechanical analyzer (DMA, SDTA861^e). The viscoelastic properties were measured from 20 ^{o}C to 190 ^{o}C under a nitrogen atmosphere, at a heating rate of 2 ^{o}C/min and frequency of 1 Hz.

Heat distortion resistance tests were carried out in an oven at different temperature (45 ^{o}C, 75 ^{o}C and 105 ^{o}C). Samples were molded in an injection molding machine (Thermo-Haake Minijet II) and then were put in the oven for 15 minutes with a

weight of 200 g hanging in the bottom. The final length of samples was measured.

Differential Scanning Calorimeter (DSC) analyses were run using a Perkin Thermal Analysis (Pyris 1 DSC) instrument. Samples (5 mg) were loaded in aluminum pans, and tests were performed under nitrogen flow of 50 ml/min. For non-isothermal melt crystallization, the sample was heated to 190 at a rate of 20 ^{o}C/min, held for 3 min to erase any thermal history, and cooled to 20 ^{o}C at a rate of 5 ^{o}C/min. The crystallization peak temperature was read from the cooling process. For isothermal melt crystallization, the sample was heated to 190 at a rate of 20 ^{o}C/min, held for 3 min to erase any thermal history, cooled to the chosen crystallization temperature at a rate of 40 ^{o}C/min, and held for a period of time until the isothermal crystallization was complete. The crystallization temperatures chosen in this work was 127 ^{o}C. The evolution of heat flow with crystallization time was recorded during the isothermal crystallization process for the later data analysis.

An optical microscope (Olympus BX51) equipped with a temperature controller (Linkam THMS 600) was used to investigate the spherulitic morphology of neat PLLA and the PLLA/KH792-RGO nanocomposites. The samples were first annealed at 190 ^{o}C for 3 min and then cooled rapidly to 146 ^{o}C.

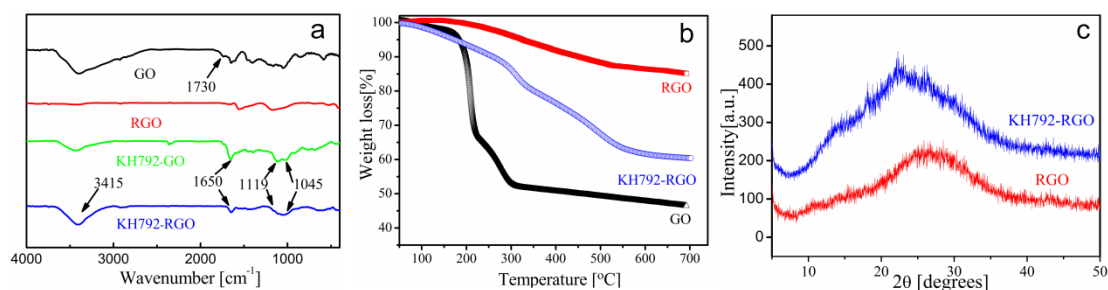## 2. Characterization of the functionalized RGO

Fig. S1 (a) FTIR spectra of GO, KH792-GO, RGO and RGO792, (b) TGA analysis of

GO, RGO and KH792-RGO, (c) X-ray diffraction patterns of RGO and KH792-RGO.

Fig. S1(a) showed the portion of amplificatory FTIR spectra of GO, RGO and KH792-RGO. The FT-IR spectrum of GO showed a C-O stretch at 1074 cm^{-1}, a broad O-H stretch at 3100-3600 cm^{-1} as well as a C=O stretch at 1730 cm^{-1}, which was in accord with previous report[3]. In the FTIR spectrum of RGO, the peaks at 1730 cm^{-1} (C=O) and 3100-3600 cm^{-1} (O-H) disappeared, suggesting that the GO was successfully reduced. In the FTIR spectrum of KH792-RGO, the absorption peak at 1045 cm^{-1} representing the Si–O–C bond and the peak at 1119 cm^{-1} representing the Si-O-Si bond appeared, indicating the successful introduction of KH792. The peak emerging at 1650 cm^{-1} was characteristic of the C=O stretch in the amide group[4], which was not found in the spectrum of RGO. The peak at 3415 cm^{-1} was attributed to N–H stretching[5]. These results demonstrated that KH792 were covalently bonded to RGO, and it was introduced through the amidation with the carboxyl groups of GO.[6]

Fig. S2(b) showed the TGA curves of GO, RGO and KH792-RGO. The TGA pattern of GO under nitrogen revealed two evident mass losses, which agreed with previous report.[7] The thermostabilization had been much improved after the successful reduction of GO. Compared with RGO, the KH792-RGO showed more weight loss, which was caused by the pyrolysis of KH792. Hence, the successful covalent functionalization of RGO sheets with KH792 was also reflected in TGA curves.

The powder X-ray diffraction (XRD) pattern of KH792-RGO was compared with that of RGO depicted in Fig. S2(c). The RGO displayed a wide diffraction peak at

$2\theta = 26.5°$, corresponding to the diffraction plane of (002) with the interlayer spacing of 0.336 nm, consistent with a well crystallized structure of graphite powders.[8] KH792-RGO showed a relatively broaden diffraction peak centered at $2\theta = 23°$. The corresponding interlayer spacing was 0.384 nm, which was larger than that of RGO, suggesting that the KH792 were successfully inserted into the sheets of RGO. The improved interlayer spacing could facilitate their uniform dispersion in appropriate organic media or polymer matrix.[9]

X-Ray photoelectron spectroscopy (XPS) was employed to further explore the interactions between RGO and KH792. Fig S2 showed the survey data of the samples and the higher resolution spectra of the Si2p, O1s, and C1s areas, respectively. The XPS spectra were collected on RGO and KH792-RGO dry powders. The survey of RGO (Fig. S2(a)) showed the absence of any detectable amounts Si (strongest XPS band was Si2p usually found between 95 and 110 eV depending on the chemical environment) and N1s (strongest XPS band was N1s usually found between 400 and 407 eV depending on the chemical environment). Compared with RGO, the survey of KH792-RGO (Fig. S2(b)) showed the presence of Si2p and N1s originating from KH792. The atom composition of N and Si element in KH792-RGO were 11.42% and 10.74% respectively (Table 1). These indicated that the graphene was successfully functionalized by KH792.
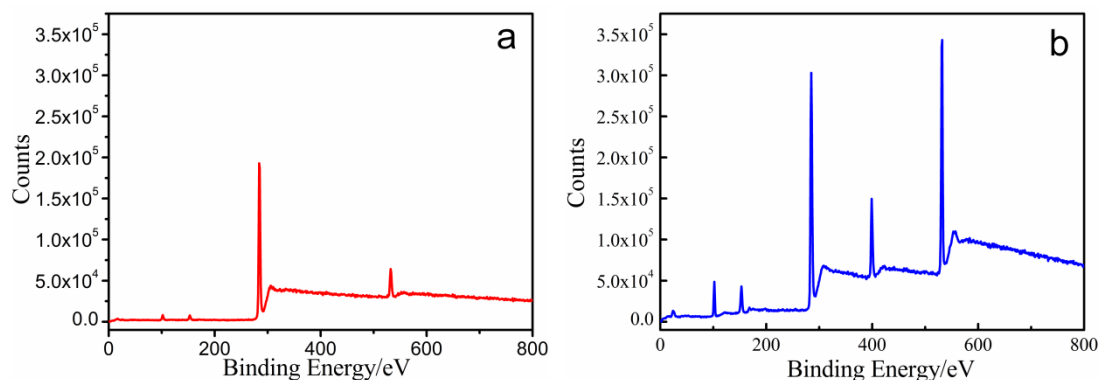
Fig. S2 The survey curves of RGO (a) and KH792-RGO (b).

Table 1 Elementary composition of KH792-RGO

Element	Peak	Atom composition (%)
C	1s	51.89
O	1s	25.96
N	1s	11.42
Si	2p	10.74

3. Crystallization behavior

There was a close relationship between the degree of crystallinity and the storage modulus of semi-crystalline polymers. In order to investigate the effects of KH792-RGO on the crystallization of PLLA, the crystallization behavior was studied. Non-isothermal and melt crystallization with cooling rate of 5 ^{o}C/min of neat PLLA and the nanocomposites was performed. As shown in Fig. S3(a), neat PLLA showed a melt crystallization peak temperature (T_{cc}) at around 113.0 ^{o}C with crystallization enthalpy (ΔH_{cc}) around 39.3 J/g, and the values of degree of crystallinity (W_c) was determined to be 45.3%; however, T_{cc} values shift gradually to 115.5 ^{o}C with the addition of 0.1 wt % KH792-RGO, and the values of ΔH_{cc} were around 42.0, 43.3 and

42.8 for PLLA/KH792-RGO-0.1%, PLLA/KH792-RGO-0.2% and PLLA/KH792-RGO-0.5% respectively. The values of W_c were determined to be around 48.4%, 49.9% and 49.3%, respectively. It was clear that T_{cc} increased apparently in the nanocomposites than in neat PLLA, as well as the ΔH_{cc} and W_c. Higher degree of crystallinity would result in higher storage modulus.
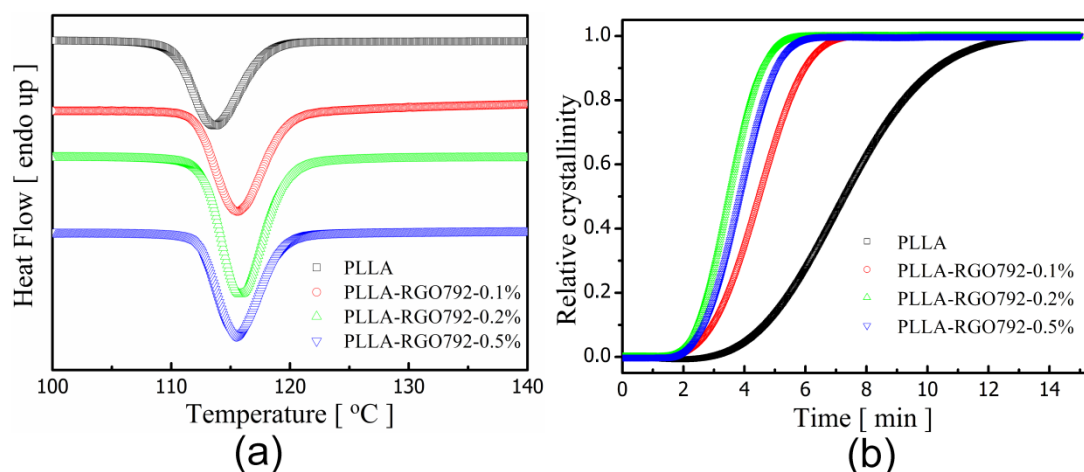

Fig. S3 (a) Non-isothermal melt crystallization with cooling rates 5 ^{o}C/min and (b) isothermal melt crystallization at 127 ^{o}C of neat PLLA and the nanocomposites.

The effect of KH792-RGO on the isothermal melt crystallization kinetics of PLLA in the nanocomposites was also investigated. The isothermal crystallization kinetics was studied at 127 ^{o}C. Fig. S3(b) showed the plots of relative crystallinity against crystallization time. It was clear that all these curves had similar sigmoid shape, but the corresponding crystallization time for the PLLA/KH792-RGO nanocomposites become shorter with increasing the KH792-RGO loading. It was obvious that the incorporation of KH792-RGO enhanced the isothermal melt crystallization of PLLA remarkably compared with neat PLLA. With enhanced crystallization rate, the storage modulus of the PLLA/KH792-RGO nanocomposites increased faster than neat PLLA.

Fig. S4 displayed the spherulitic morphology of neat PLLA and the nanocomposites crystallized at 127 °C. As shown in Fig. S4(a), the well-developed spherulites of neat PLLA grew to a size of about 150 μm in diameter, and the boundaries were clear. Fig. S4 (b, c, and d) illustrated the polarizing optical microscope (POM) images of the nanocomposites with the KH792-RGO loading from 0.1 to 0.5 wt% respectively. It was obvious that there were more spherulites in the PLLA/KH792-RGO nanocomposites than in neat PLLA, while the size of PLLA spherulites was smaller in the PLLA/KH792-RGO nanocomposites than in neat PLLA. Such variations indicated that the nucleation density of PLLA spherulites increased in the PLLA/KH792-RGO nanocomposites because of the nucleating agent effect of KH792-RGO.
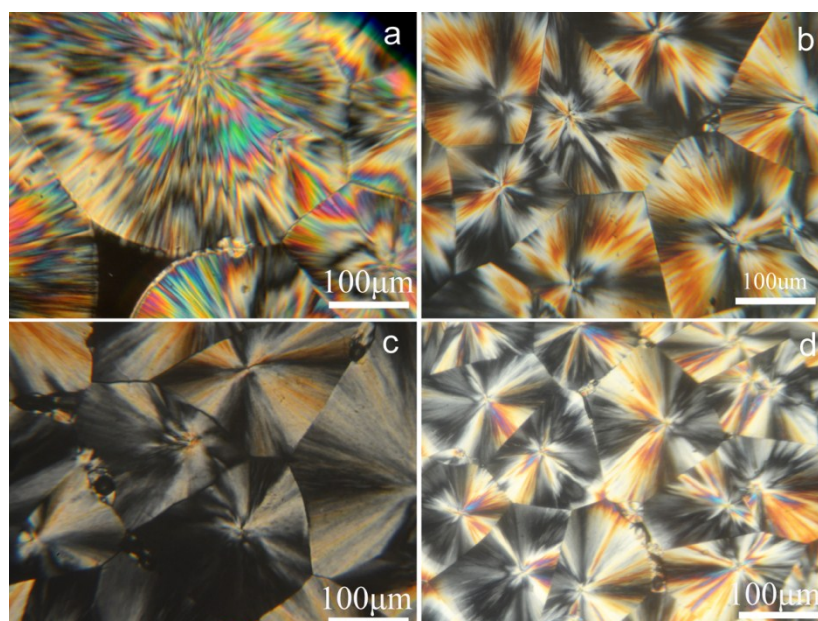

Fig. S4 POM images of neat PLLA and the nanocomposites crystallized at 127 °C for 30 min; (a) neat PLLA, (b) PLLA/KH792-RGO-0.1%, (c) PLLA/KH792-RGO-0.2%, and (d) PLLA/KH792-RGO-0.5%.

4. Heat Distortion Resistance of PLLA-POSS nanocomposites (for control).

To show the heat distortion resistance of PLLA composites with other types of filler

in the rubber state, we prepared a PLLA-POSS composite with 2 wt% of N-Phenylaminomethyl POSS according to a previous publication.[10] As shown in Fig. S5, the heat distortion resistance of PLLA-POSS-2% was only slightly varied as compared to neat PLLA.
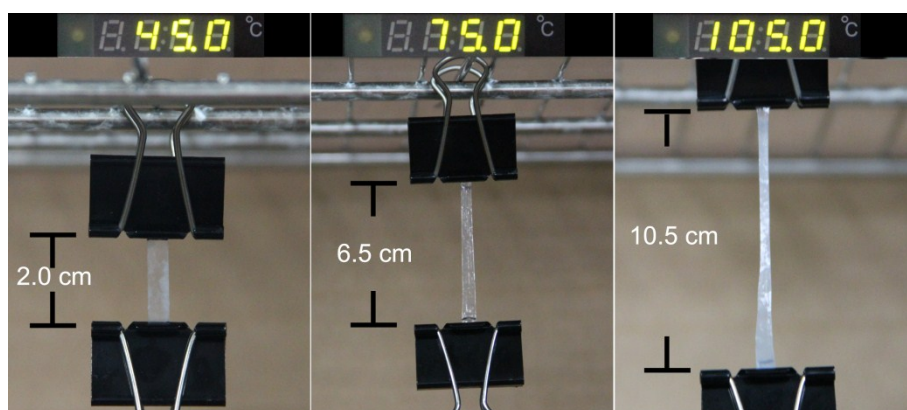

Fig. S5 Heat distortion resistance of PLLA/POSS-2% at different temperature.

1.   W. Jiang, W. Huang, N. Cheng, Y. Qi, X. Zong, H. Li and Q. Zhang, *Polymer*, 2012, **53**, 5476-5479.

2.   W. S. Hummers and R. E. Offeman, *Journal of the American Chemical Society*, 1958, **80**, 1339-1339.

3.   S. Park, K.-S. Lee, G. Bozoklu, W. Cai, S. T. Nguyen and R. S. Ruoff, *ACS Nano*, 2008, **2**, 572-578.

4.   L. Lai, L. Chen, D. Zhan, L. Sun, J. Liu, S. H. Lim, C. K. Poh, Z. Shen and J. Lin, *Carbon*, 2011, **49**, 3250-3257.

5.   H. Cao, X. Wu, G. Yin and J. H. Warner, *Inorganic Chemistry*, 2012, **51**, 2954-2960.

6.   T. Huang, R. Lu, C. Su, H. Wang, Z. Guo, P. Liu, Z. Huang, H. Chen and T. Li,

ACS Applied Materials & Interfaces, 2012, **4**, 2699-2708.

7.   M. J. McAllister, J.-L. Li, D. H. Adamson, H. C. Schniepp, A. A. Abdala, J. Liu, M. Herrera-Alonso, D. L. Milius, R. Car, R. K. Prud'homme and I. A. Aksay, *Chemistry of Materials*, 2007, **19**, 4396-4404.

8.   G. Wang, X. Sun, C. Liu and J. Lian, *Applied Physics Letters* 2011, **99**, 3.

9.   Y. Cao, J. Feng and P. Wu, *Carbon*, 2010, **48**, 3834-3839.

10. Q. Zhang, H. He, K. Xi, X. Huang, X. Yu and X. Jia, *Macromolecules*, 2011, **44**, 550-557.